Available online at www.sciencedirect.com

jmr&t Journal of Materials Research and Technology

www.jmrt.com.br

Original Article

The role of graphite addition on spark plasma sintered titanium nitride

O.J. Akinribide[a,b,*], B.A. Obadele[a,c], O.O. Ayeleru[a], S.O. Akinwamide[a], K. Nomoto[b], M. Eizadjou[b], S.P. Ringer[b], P.A. Olubambi[a]

[a] Centre for Nanoengineering and Tribocorrosion, School of Mining, Metallurgy and Chemical Engineering University of Johannesburg Doornfontein Campus, Johannesburg, South Africa

[b] Australian Centre for Microscopy and Microanalysis, School of Aerospace, Mechanical Mechatronic Engineering The University of Sydney, NSW 2006, Australia

[c] Department of Chemical, Materials and Metallurgical Engineering, Botswana International University of Science and Technology, Palapye, Botswana

ARTICLE INFO

Article history:
Received 18 January 2020
Accepted 10 March 2020
Available online 27 April 2020

Keywords:
TiN
Graphite
Spark plasma sintering
Microstructure

ABSTRACT

Composites of titanium nitride reinforced with graphite were synthesized using spark plasma sintering at 2000 °C. The effects of graphite addition on the microstructure, relative density, and mechanical properties of TiN ceramics matrix were examined. The investigation was performed on TiN powder with varying graphite content (1–5 wt.%) for 8 h using an energy ball milling equipment. Results show that TiN without and with graphite (TiN + 1 wt.% graphite) sintered at 2000 °C recorded sintered relative density of 96.7% and 97% respectively. Additionally, TiN with 3 wt.% graphite had a relative density of 98%. However, the shrinkage of TiN + 3 wt.% graphite was observed to be the lowest compared to other composites at the same sintering conditions. Microstructural analysis indicates that the grain of titanium nitride in the composite was very fine and continuous. Subsequently, a bimodal particle sizes were observed when 5 wt.% graphite was dispersed in TiN. The highest Vickers microhardness of 23.5 GPa and fracture toughness of 6.5 MPa $m^{1/2}$ were achieved with composites reinforced with 3 wt.% graphite at milling period of 8 h. The combination of TEM/EDS and HRTEM/FFT show a single pattern of diffraction and consistency in interplanar distance obtained from X-ray diffractometry of the milled sample. There is a clear coherence interface between the phases.

1. Introduction

Titanium nitride (TiN) is an important covalent ceramic material that is widely recognized as the most captivating engineering ceramic materials due to its high thermal and electrical conductivities, high melting point (about 3200 K), low coefficient of friction, good chemical stability and corrosion resistance [1,2]. Graphite as a carbon-based material in this study is regarded as a good inhibitor to the formation of intermetallic binder compounds and proffer the risk of enhanced properties to the cermet. Graphite in view of its great financial values is effectively accessible and generally referred to as a

* Corresponding author.
E-mail: akinribideojo@yahoo.com (O. Akinribide).

https://doi.org/10.1016/j.jmrt.2020.03.040

solid lubricant as well as commodity mineral. Graphite could serve as a good material in the manufacture of self-lubricating tools in powder metallurgy. On account of the excellent properties of TiN and graphite, there applications can be found in Jet motor parts, cutting tools, milling, sectioning, boring, etc. [3]. However, because of high melting point and low degree of diffusion of titanium nitride and graphite, TiN and graphite are hard to sinter as composites. Few articles are available on TiN–graphite composites fabrication via powder mixing (in a Turbula Shaker Mixer) and thereafter sintering using a conventional sintering procedures, for example, hot pressing or pressure-less sintering [4–8].

Compared to other conventional sintering methods available in literatures, obtaining a very dense sintered composites have been ascribed to the utilization of spark plasma sintering (SPS) on account of reducing grain growth in the composite structure, which could later offer the best mechanical properties of the sintered cermet. Among spark plasma sintering processes, a pulse DC could be provided to a conductive die and the admixed powders. The admixed powders present within the die are consistently heated all around. TiN–TiB_2 composite is conceivably sintered by spark plasma sintering just like other ceramic composites that cannot be completely densified by common conventional sintering processes [9]. Reactive spark plasma sintering of TiN–TiB_2 composites with different proportion of TiH_2, BN, B and TiN were beforehand reported by Khobta et al. [10] and Petukhov et al. [11]. However, in view of its exothermic response, a completely dense body could not be acquired. Furthermore, high dense sintered TiN–TiB_2 composites were acquired by hot-pressing at high temperatures. Nonetheless, prolonged sintering time is required which could result in the development of grain growth and bring about poor mechanical properties. On the other hand, conventional sintering techniques have been utilized to sinter submicron size titanium nitride, which resulted in low densification [12–15]. Additionally, the development of grains within the microstructure of the sintered TiN contributes to the weakness observed in the mechanical properties of any ceramic materials [10]. In other to improve the mechanical properties of ceramic materials, several reinforcing materials such as metal binders (iron (Fe), nickel (Ni), cobalt (Co), etc.), nitrides, carbide, oxides and hydrides of several elements and compounds have been used to reinforced ceramic matrix materials according to [16–19]. From literature, it was discovered that an improved mechanical properties of any ceramic matrix composites could only possible with inclusion of secondary phase in the cermet [20]. Compared to any other sintering techniques, spark plasma sintering has been generally accepted because of its several advantages and its capacity to sinter with minimum deficiencies, little holding time, good thermal stability and high temperature for short range of time [10,21–29].

Notwithstanding, a few studies have been done on the improvement of sintering techniques, densification and mechanical properties of titanium nitride. However, there are a few difficulties encountered in order to fabricate a technological proven TiN ceramic without binders. Uncontrollable growth of grains in the developed TiN based ceramics composites has been a major problem. This major problem serves as a challenge for researchers to analyze different techniques to determine the current existing issues of such ceramics.

Table 1 – Details of as-received powders and specifications.

Matrix	TiN
Manufacturer	>99 wt.% purity (600140 from China)
Average particle size	1.15 μm size, 3 kg net weight
Reinforcement	Graphite
Average particle size	1.2 μm
Manufacturer	Sigma–Aldrich, South Africa

Some studies have shown that the relative density of approximately 99% is possible for titanium reinforced with titanium diborides. Uniaxial pressure of 35 MPa was applied for a period of 10 min and thereafter sintered at 2100 °C [30]. Khobta et al. [10] reported poor mechanical properties for titanium diboride (TiB_2) when sintered at heating rate between 112.5 and 300 °C/min. Kitiwan et al. [31,32] also obtained high hardness and fracture toughness (20.1 GPa and 4.3 MPa $m^{1/2}$, respectively) when TiN is reinforced with TiB_2 and hBN [31,32]. Some additives such as hexagonal boron nitride, TiB_2 and titanium oxides have been used to reinforce TiN in order to improve their thermomechanical properties [32–36].

The present investigation study the sintering behaviours of TiN based cermets reinforced with graphite. The influence of graphite on the sintering parameters, microstructure, phase change and mechanical properties such as hardness and fracture toughness were examined.

2. Experimental

Titanium nitride (TiN) and graphite powders were utilized as presented in Table 1. TiN powder served as a matrix with graphite powder as reinforcement. Four varying compositions of TiN and graphite powders were developed (pure TiN, TiN + 1 wt.% graphite, TiN + 3 wt.% graphite and TiN + 5 wt.% graphite) and milled for 8 h in a high energy ball mill (HEBM Retsch PM 400, Germany) using WC balls (with ethanol as milling medium) at a ball to powder ratio of 10:1 and speed of 250 rpm. Vacuum extractor was used to dry the sample for 2 h at 80 °C.

The milled powders were then consolidated in a 20 mm diameter die via spark plasma sintering (model HHPD25, FCT Germany) at 2000 °C, sintering rate of 100 °C/min, applied pressure of 50 MPa and holding time of 900 s. The thickness of each sample after sintering was 4.5 mm. The straight shrinkage of the samples amid sintering were observed by dislodging a punch pole [37]. The values of the apparent density were estimated utilizing the Archimedes technique, and the relative density was ascertained from the hypothetical density of TiN (5.4 g cm^{-3}) and graphite as (2.2 g cm^{-3}).

The phases present before and after sintering were analyzed by X-ray diffractometry (PANalytical Empyrean) with Cu-Kα radiation. Microstructures were obtained by utilizing a field emission scanning electron microscope at 10 kV using FE-SEM JSM-7600F. The detail analysis of the milled powders was further characterized by high resolution Transmission electron microscopy (HRTEM) using FEI Themis-Z

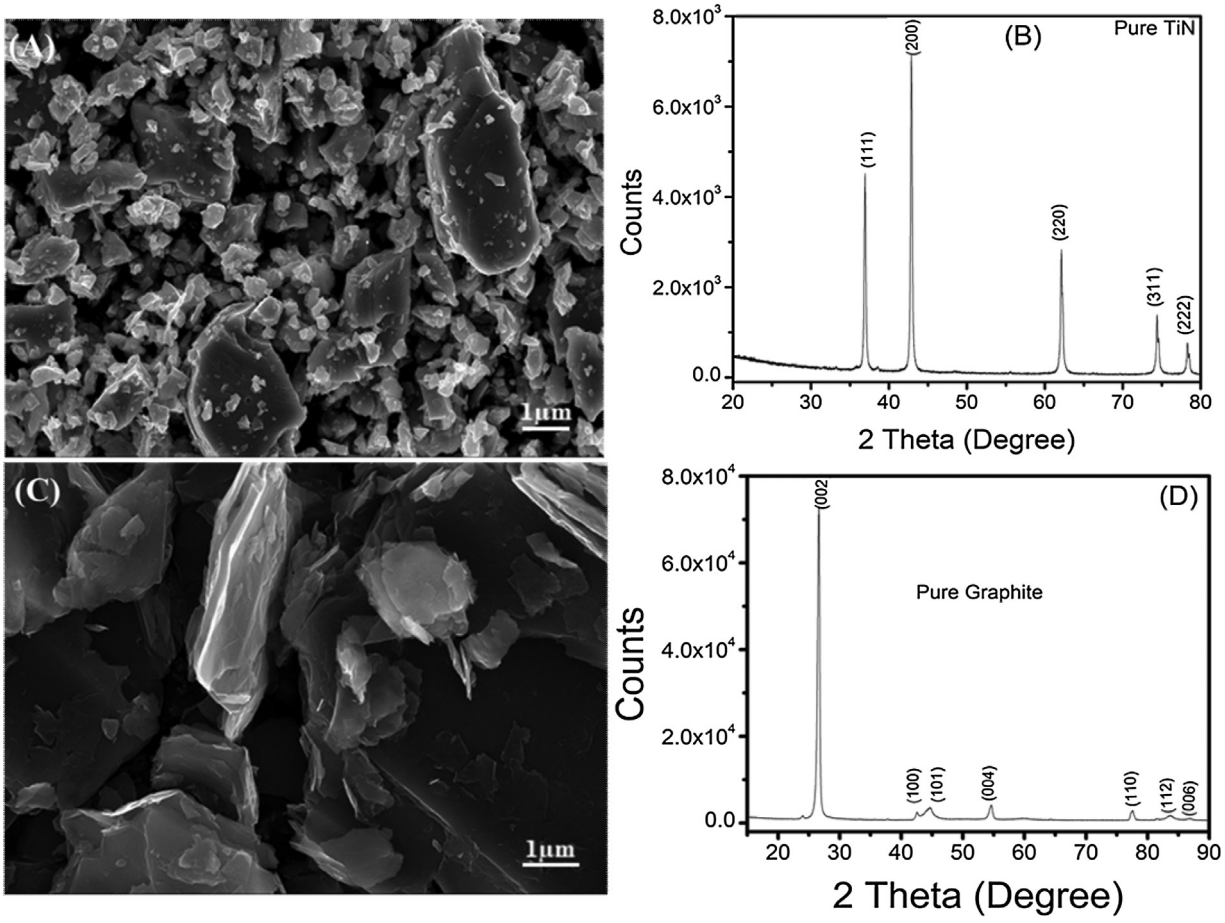

Fig. 1 – SEM morphologies and corresponding XRD patterns of (a, b) pure TiN and (c, d) pure graphite.

Double-corrected 60–300 kV S/TEM at University of Sydney nanoscience hub. After mounting, the microstructural analysis of the sintered samples was investigated using SEM with model (JEOL JSM-7600F) equipped with EDS known as energy dispersive spectroscopy. The microhardness together with the fracture toughness were carryout using microhardness tester (FALCON 500 series) to determine the average Vickers micro indentation hardness and fracture toughness after five repeated experimental values at a load of 1 kgf [1,7].

3. Results and discussion

3.1. SEM and phase analysis of as-received powders

Fig. 1a illustrates the SEM morphologies of TiN powders with a randomly distributed particles and average particle size less than 2.0 μm while the natural flake graphite powder (see Fig. 1c) has a flake-like morphology. The XRD patterns of the starting powders are shown in Fig. 1b and d. The crystalline phases detected in Fig. 1b are typical of pure TiN.

The highest intensity peak for TiN powder was identified at peak position of $2\theta = 42.6^\circ$ which correspond to (200) plane, followed by other peaks at $2\theta = 36.6^\circ$, 61.8°, 74.1° and 77.9°, which correspond respectively to (111), (220), (311) and (222) planes of TiN. The highest peak intensity of $2\theta = 26.6^\circ$ was observed for graphite corresponding to (002) plane [1,38]. Other peaks are located at $2\theta = 44.3^\circ$ and 54.5° corresponding to planes (101) and (004) respectively.

3.2. SEM and XRD analysis of the milled powders

Fig. 2 shows the SEM morphologies of milled TiN with different proportions of graphite (1–5 wt.%). It could be seen that the powders display particles of different shapes and sizes. Also, the milled powders display some degree of agglomeration after milling for 8 h with some irregular, flaky and spherical morphologies which resulted in spongy appearance.

Likewise, there is a reduction in particle size of the powders after milling for 8 h when compared with pure TiN without (in Fig. 1a) and with graphite additions as shown in Fig. 2a, c and e.

From the X-ray pattern of the milled powders as shown in Fig. 2b, it was observed that similar peak positions of $2\theta = 42.6^\circ$, 36.6°, 61.8°, 74.1° and 77.9° were detected which is quite similar to as-received pure TiN and FCC $TiC_{0.3}N_{0.7}$. This steady state in diffraction angles at $\approx 43^\circ$ shows that all the samples exhibit the same lattice parameters due to dissolution of carbon (C), nitrogen (N) and titanium (Ti). According to recent work done by Takamori et al. [39], titanium alloys can only accommodate the maximum solubility of 0.2 at.% carbon. This percentage is observed to be conspicuously lesser than the percentage

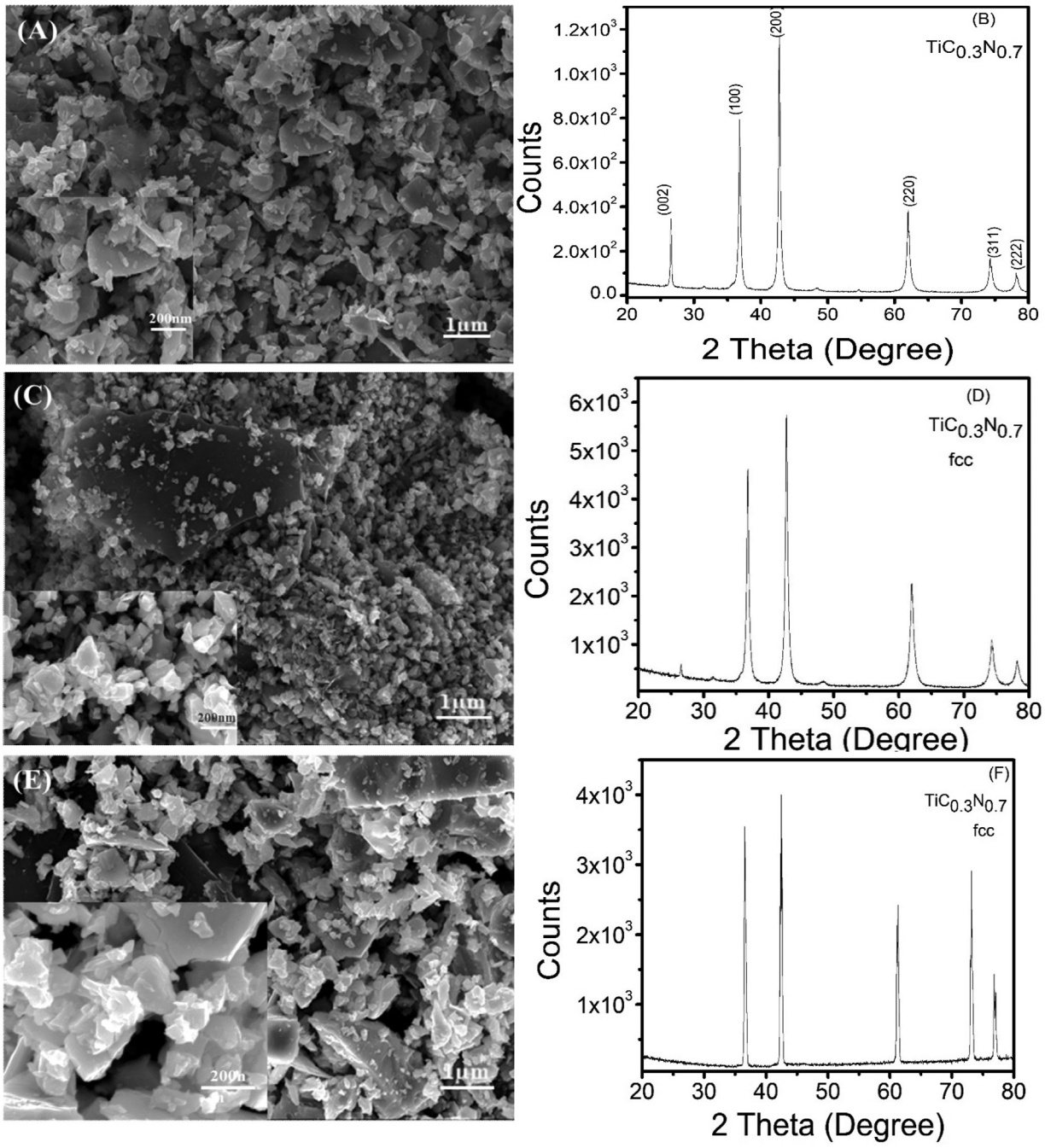

Fig. 2 – SEM micrographs and corresponding XRD patterns of the milled samples (a, b) TiN + 1 wt.% graphite, (c, d) TiN + 3 wt.% graphite and (e, f) TiN + 5 wt.% graphite.

of graphite used in reinforcing the titanium nitride matrix in this study. As a result of the clear crystallinity of the milled powder, carbon (graphite) peaks were retained and there is no observable shift in the atomic scattering factors of titanium nitride which agrees with Lohse et al. [40] and Ye and Quan [41]. It has been noticed that a decrease in the peak's intensity of titanium carbonitride as the percentage composition of graphite increases in Fig. 2b, d and f. Moreover, all the diffraction peaks position was observed to be in good conformity with NaCl rock salt crystal type faced centre cubic (FCC) phase. This phenomenon was achieved as a result of decomposition of ethanol as the process control agent when allowed to react with TiN in the milling vials, also the reaction that exist among (carbon C, nitrogen N, and titanium Ti).

Dorofeev et al. [42] reported the formation of a completely stabled titanium carbide when TiC_xH_y was heated in a vacuum [42]. Changing the milling time has been confirmed as the important milling parameters necessary for milling titanium in toluene as the principal component analysis (PCA) to form carbon to titanium ratio by [43]. There is also a documented evidence that an in situ titanium carbide formation is possible when milling titanium and carbon because of diffusion

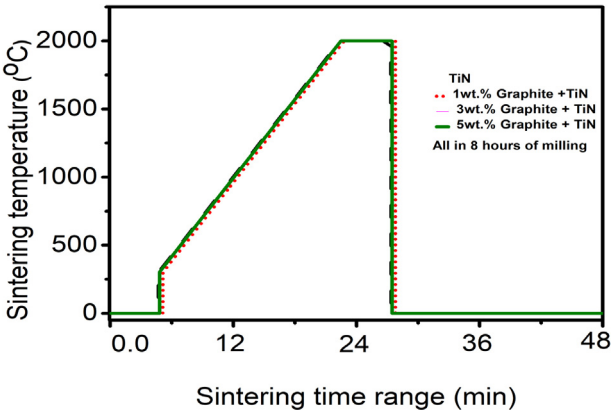

Fig. 3 – Sintering temperature against sintering time for sintered TiN without and with 1–5 wt.% graphite additions.

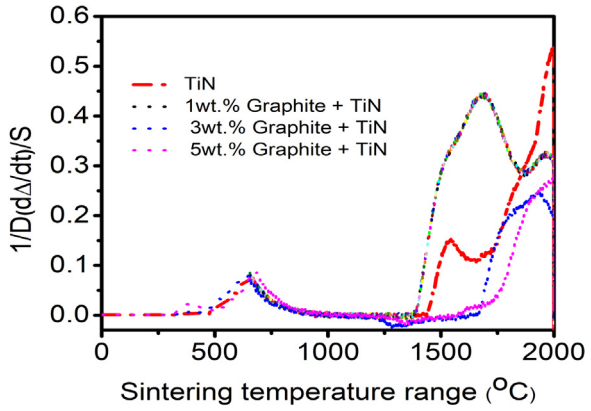

Fig. 4 – Densification rate of sintered TiN without and with 1–5 wt.% graphite additions.

propagated by mechanical induced self-propagating reaction [44]. In this experiment, the milling in wet condition was investigated so there are no signs of any high adiabatic temperature involved in the reaction at room temperature, which could be possible in dry milling [45–48]. The focus of this study is to produce TiCN of different C/N ratio that will give the optimum level of toughness for high speed cutting tools application without the application of any metallic binders. Generally, TiN, TiC, TiCN and TiAlN have similar peak positions [49–53].

3.3. *Densification behaviours and microhardness values*

Fig. 3 shows the sintering temperature against sintering time on the sintered TiN-graphite composites at 2000 °C. An applied pressure of 50 MPa was maintained all through the sintering regime. Firstly, the graphite die was pre-heated from 0 °C to about 250 °C and thereafter, incresed steadily to 2000 °C at a constant heating rate of 100 °C/min. At the peak temperature (i.e. 2000 °C), the temperature was held for about 10 min. Generally, the sintered composites display similar trend in the sintering temperature profile.

Fig. 4 presents the rate of densification of the sintered composites. The parameters used in determining the rate of densification of the sintered samples are as follows;

$$þ_{rp} = \left[\frac{þ_{ind/ts}}{þ_{fd} - þ_{ind}}\right] \quad (1)$$

where $þ_{rp}$ = is the densification rates parameters, $þ_{ind}$ = is the initial density of the composite, $þ_{fd}$ = is the final density of the composite and t_s = sintering time

Fig. 4 shows that the rate of densification of the composites commenced from 650 to 1700 °C. The displacement of titanium nitride–graphite composites follow the same trends, expecially within the temperature range of 1000–1800 °C [11]. It was observed that the rate of densification increases at 1 wt.% graphite and later decreases as the percentage weight of graphite content increases in the titanium nitride, which is a clear indication of difficulty encountered while sintering titanium nitride with an increase in carbon content. This is also in support of the statement "the densification of titanium alloys improves by lowering the C/TiN ratio" despite reducing the volumemetric shrinkage due to conversion of titanium carbonitride. The sample with 1 wt.% graphite demonstrate the highest rate of densification at 0.45 °s^{-1} as seen in Fig. 4 followed by sample with 5 wt.% graphite at 0.25 s^{-1} and 3 wt.% graphite at 0.23 °s^{-1}. The highest rate of densification was obtained at 0.51 s^{-1} for pure titanium nitride matrix. The lowest rate of densification experienced by other composites could be as a result of segregated graphite in the titanium nitride which is clearly seen as pores and undissolved carbon in the microstructure in Fig. 7.

The optimum shrinkage observed in the compositions investigated in Fig. 4 could be attributed to constant heating rate of 100 °C/min as well as the graphite content in the sintered ceramic composites. The exothermic reactions taking place in between the Ti and N atom could also contribute to self-heating of the ceramic composites which in the end lead to structural development or formation of structures in the ceramic composites. Therefore, ceramic composites containing 1 wt.% graphite have the higher optimal shrinkage in contrast to TiN ceramic composite containing 3 and 5 wt.% graphite. This is due to present of carbon (graphite) and nitrogen as an exceptional lubricant right from the milling stage of the powders. Classically, at the temperature of 1500 °C the ceramic composites with 3 wt.%graphite and 5 wt.% graphite decreases more compared to 1 wt.% in Fig. 4. Seemingly, for the densification of ceramic composite containing 3 and 5 wt.% to be complete, there is need for higher sintering temperature or simply prolong holding time for complete densification to form. Further extension in the graphite content from 6 to 7 wt.% could lead to breaking of graphite die as a result of transient thermal destruction within the spark plasma sintering machine at higher temperature.

The relative density of the sintered composites is shown in Fig. 5. Addition of graphite to TiN had a mixed influence on the relative density attained by each composite. For 1 and 3 wt.% graphite additions, the relative densities were 97% and 98% respectively. This could be as a result of graphite presence within the sintered compacts voids/pores. The relative

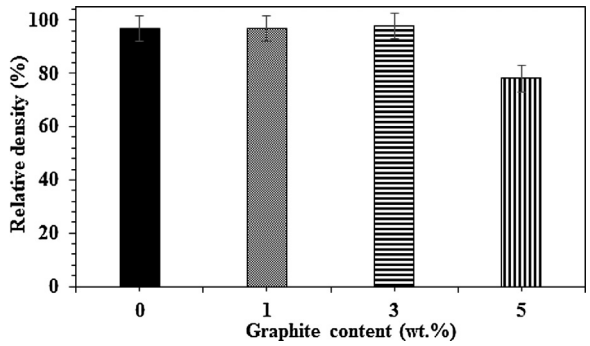

Fig. 5 – Relative density against the percentage weight of graphite in 1–5 wt.% graphite (the error bar is the standard error based on five repeated experiment for each data points).

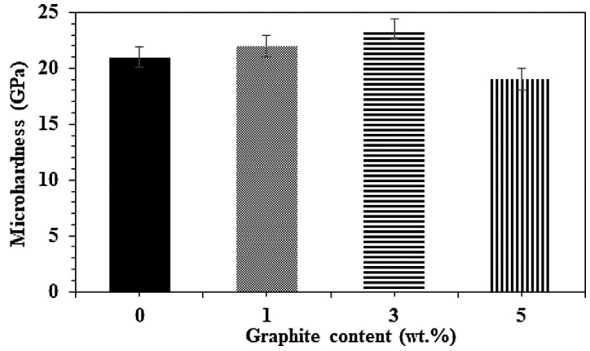

Fig. 6 – Microhardness values against percentage weight of graphite in 1–5 wt.% TiN (the error bar is the standard error base on five repeated experiment for each data points).

density of the pure titanium nitride is 96.7% indicating the effeciency of the spark plasma sintering technique on the developed composites at 2000 °C. Generally, it could be seen that there is a slight increase in the relative density of the sintered composite reinforced with 1 and 3 wt.% graphite in titanium nitride-based ceramic composites compared to titanium nitride without reinforcement.

Fig. 6 presents the microhardness values obtained for sintered TiN composites without and with graphite additions. Generally, the hardness values increase as the graphite content increase up to 3 wt.% graphite addition. The hardness values of pure TiN with 1–3 wt.% graphite at sintering temperature of 2000 °C are 21, 22 and 23.5 GPa at relative density of 96.5%, 97% and 98% respectively. However, for 5 wt.% graphite, it is clearly seen that the microhardness value significantly drop to 19 GPa. It could be stated that increasing the graphite contents above 3 wt.% in TiN could decrease the hardness of the composite. This could be attributed to the low hardness nature of graphite which is present as agglomerates or along the grain boundaries of TiN matrix.

3.4. *SEM and phase analysis of the sintered composites*

Fig. 7 shows the SEM images and corresponding XRD of the sintered composites without and with graphite additions. From the micrographs, the grey areas represent TiN while the dark areas could be presented as the graphite respectively. Graphite dominated the entire region as dark phase in the micrographs which symbolized the secondary phase in the developed composite and observed to be uniformly distributed along the grain boundary with a more progressively homogenous microstructure. It could be observed from Fig. 7c, e and g that an increase in percentage composition of graphite after milling for 8 h and sintering at 2000 °C reduced the densification of the developed composites significantly which is confirmed in Fig. 5. It could be seen that very small amount of graphite phase is present within the TiN matrix forming an interfacial reaction. Most of the graphite are found within the grain boundaries and thereby restraining the widespread grain growth in the microstructures.

At sintered temperature of 2000 °C, the grain shape was round or granular with little or/no observed pores, demonstrating adequate densification. At the same sintering temperature of 2000 °C, as shown in Fig. 7, TiN grains was partially expanded by grain growth, while few grains were flattened and circular in shape and the grain size turned out to be considerably higher than that of the starting powder due to milling time of the powders. Grain growth with a polygonal shape can be seen as the graphite contents increases. A large pulse current flow in SPS process could have potential field impacts at particles contacts, i.e., high local temperature slope by Wan et al. [1] and Chicardi et al. [38] and upgrade of mass transport [54] which would bring about a fast consolidation. The complex texture containing little TiN grains might be due to earlier phase of eutectic nature of TiN–graphite composite where the structure begins to shape core and rim phase. A similar texture was observed in eutectic matrix in the composite sintered by SPS [37].

XRD patterns in Fig. 2b, d, and f show complete formation of TiCN phase in the TiN-graphite composites. The diffraction angles of each peak remain at their respective 2θ degree positions before sintering as shown in Fig. 2. There is a sharp peak in the diffraction angle 2θ in Fig. 7f for each spectrum compared to Fig. 7b and d. This was reported in previous research study on the microstructural and phase evolution of spark plasma sintered graphitized Ti $C_{0.9}$ $N_{0.1}$ [55]. The highest peak intensities were obtained in Fig. 7f, all in accordance with (100), (110), (100) and (200) planes. The structural arrangement depends mainly on the relationship between carbon/nitrogen.

On the other hand, it could be seen that most of the diffractions peaks are mainly TiCN with no significant graphite peak. The carbon atoms within the matrix act as a source of interference as diffraction occurs in plane (110). Therefore, increase in the graphite content automatically leads to a slight reduction in the peak intensity of plane (110). In addition, the planes corresponding to the index (111) has the highest peak in Fig. 7f.

3.5. *TEM/EDS mapping of the milled powder*

Fig. 8a shows the HAADF/TEM image of the composite with 3 wt.% graphite in titanium nitride which is obviously the composite with the highest sintered density. The dark region of the micrograph is rich in graphite while the region with bright appearance is the TiN phase. The image in Fig. 8b presents a clear HRTEM (high resolution TEM) image of the spot coloured

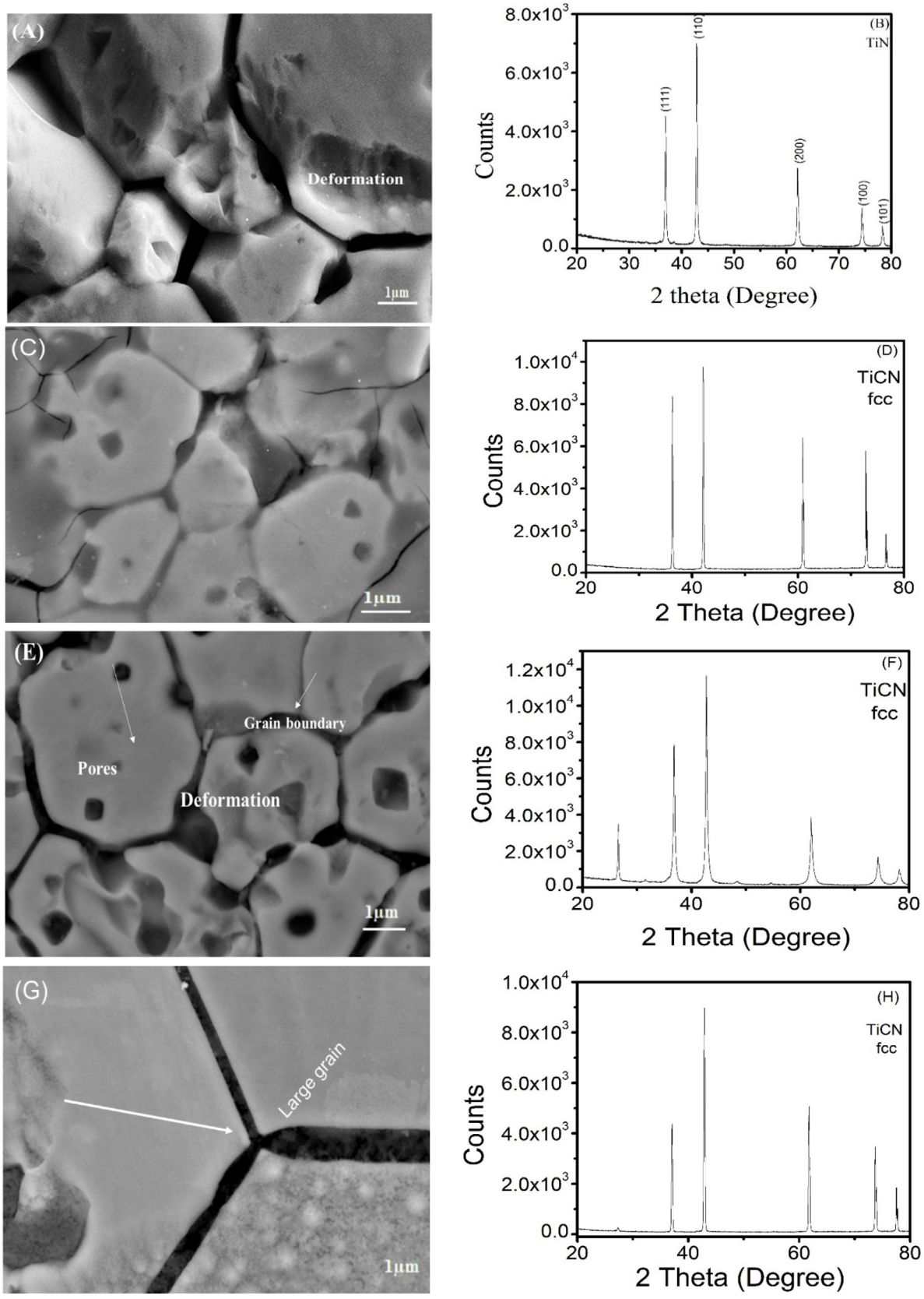

Fig. 7 – SEM micrographs and corresponding XRD of the sintered compacts: (a, b) pure TiN, (c, d) TiN + 1 wt.% graphite, (e, f) TiN + 3 wt.% graphite and (g, h) TiN + 5 wt.% graphite.

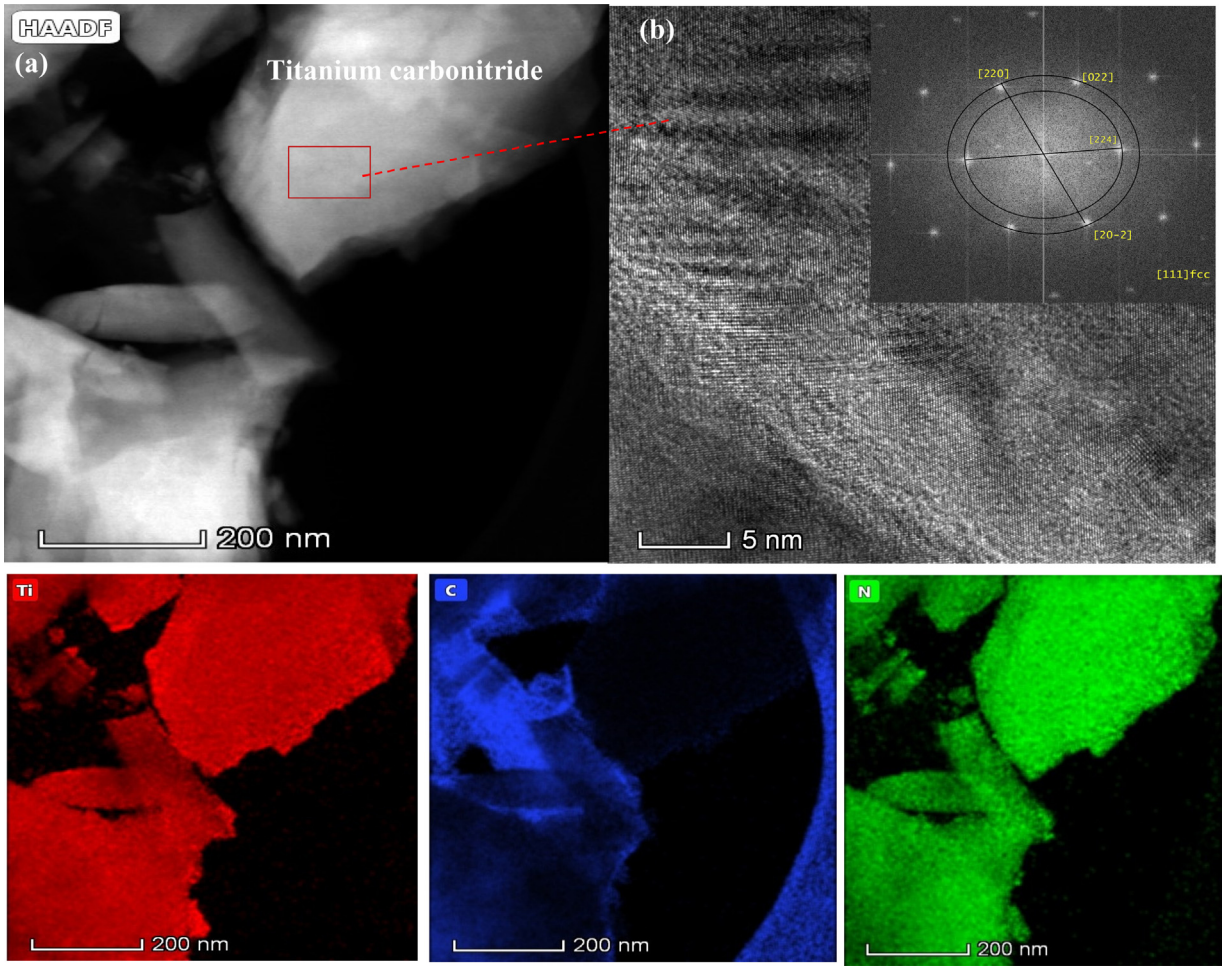

Fig. 8 – (a) HAADF/EDS mapping of 3 wt.% graphite powder and (b) HRTEM/FFT of the powder.

in yellow square with the corresponding fast fourier transformed (FFT) patterns. From the image, it can be observed that there is only single pattern of diffraction without any other discontinous spot as indicated in the FFT inserts in the HRTEM image in Fig. 8b. The indexing of the lattice planes was done using the distance from the origin known as the interplannar distance in the HRTEM. The interplannar distance obtained from the X-ray difrractometer results of this study show some consistency in the interface between the dark and bright region. According to Laoui et al. [56], Rafaja et al. [57] and Cutard et al. [58], they discovered some misfit in the dislocation of the two distinct interfaces in TiCN. The inserts in Fig. 8b shows some orientation at the interface and very close to the edge of titanium carbonitride particles. The crystal orientation of the TiCN has a direction close to [220], [022], [224] and [20−2] planes. Due to the same direction of crystal, it is believed that a perfect coherent interface are developed between the graphite and titanium carbonitride particle boundaries. The sodium chloride type of titanium carbonitride is formed at the top surface layer because of the increase in the packing density [59]. Hence, it can be concluded that the high energy ball milling process has played a significant role in the development of the TiCN. Similar trend was noticed in the reseach study of Xiong

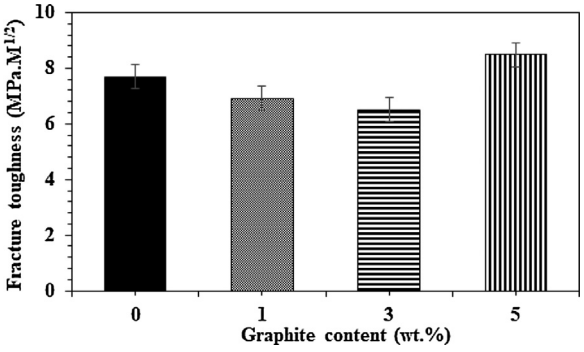

Fig. 9 – Fracture toughness against percentage weight of graphite in TiN (the error bar is the standard error based on five repeated experiment for each data points).

and Park et al. on the titanium carbonitride/Nickel interface with some orientation of planes [60]. The EDS mapping in Fig. 4 shows the uniform distribution of graphite in the titanium nitride matrix because of the process used during the milling stage of the powder. These elemental distribution could help in increasing the thermal conductivity of the composites.

3.6. *Fracture toughness of the sintered composites*

Fig. 9 shows the effect of graphite contents on the fracture toughness of the developed composites. The results shows that 1 and 3 wt.% has remarkably improved the fracture toughness of the composites but further increase of 5 wt.% graphite in the TiN matrix increase the fracture toughness to 8.5 MPa $m^{1/2}$, which indirectly weaken the mechanical properties of the composite. The fracture toughness of 6.5 MPa $m^{1/2}$ for 3 wt.% graphite in the sintered composite was better compared to pure TiN, 1 and 5 wt.% of graphite composites as shown in Fig. 9.

4. Conclusion

In this study, titanium nitride–graphite composites was fabricated by spark plasma sintering (SPS) at 2000 °C. The pure TiN and 1 wt.% graphite TiN composites displayed relative densities of 96.7% and 97% respectively. A completely densed TiN–3 wt.% graphite composites of 98% were achieved at the same sintering temperature of 2000 °C. The TiN–1 wt.% graphite composite displayed the highest densificattion rate amid the milled samples. The TiN–3 wt.% graphite composite sintered at 2000 °C have the highest hardness with fracture toughness of 23.5 GPa and 6.5 MPa $m^{1/2}$ respectively. The spark plasma sintering at sintering temperature of 2000 °C can be used to sintere a completely densified TiN–graphite composites, and results in the highest mechanical properties if the weight percent of graphite is carefully controlled.

Conflicts of interest

The authors declare no conflicts of interest.

Acknowledgements

The study is supported financially by National Research Foundation (NRF), South Africa and University of Johannesburg in South Africa. The authors also acknowledge the facilities, scientific and technical assistance of the Microscopy Australia node at the University of Sydney (Sydney Microscopy & Microanalysis). The authors are particularly grateful to Dr. Magnus Garbrecht, Vijay Bhatia and Jacob Byrnes for their technical assistance in the SEM and HRTEM.

REFERENCES

[1] Wan W, Xiong J, Liang M. Effects of secondary carbides on the microstructure, mechanical properties and erosive wear of Ti (C, N)-based cermets. Ceram Int 2017;43(1):944–52.
[2] Veprek S, Zeer A, Riedel R. Handbook of ceramic hard materials. Weinheim: Wiley; 2000.
[3] Akinribide OJ, et al. Sintering of binderless TiN and TiCN-based cermet for toughness applications: processing techniques and mechanical properties: a review. Ceram Int 2019;45(17 Part A):21077–90, http://dx.doi.org/10.1016/j.ceramint.2019.07.191.
[4] Abdellaoui M, Gaffet E. Mechanical alloying in a planetary ball mill: kinematic description. J Phys IV 1994;4(C3). C3-291–296.
[5] Liu L-Z, Ying G-B, Zhu J, Lin H, Zhu C-C. High-temperature compressive properties of TiC–TiB_2/Cu composites prepared by self-propagating high-temperature synthesis. Rare Metals 2014;33(1):95–8.
[6] Sarma B, Chandran KR. Accelerated kinetics of surface hardening by diffusion near phase transition temperature: mechanism of growth of boride layers on titanium. Acta Mater 2011;59(10):4216–28.
[7] Kitiwan M, Ito A, Goto T. B deficiency in TiB2 and B solid solution in TiN in TiN–TiB_2 composites prepared by spark plasma sintering. J Eur Ceram Soc 2012;32(16):4021–4.
[8] Lengauer W, et al. Solid state properties of group IVb carbonitrides. J Alloys Compds 1995;217(1):137–47.
[9] Shobu K, Watanabe T, Enomoto Y, Umeda K, Tsuya Y. Frictional properties of sintered TiN–TiB_2 and Ti (CN)–TiB_2 ceramics at high temperature. J Am Ceram Soc 1987;70(5). C-103–104.
[10] Khobta I, Petukhov O, Vasylkiv O, Sakka Y, Ragulya A. Synthesis and consolidation of TiN/TiB_2 ceramic composites via reactive spark plasma sintering. J Alloys Compds 2011;509(5):1601–6.
[11] Petukhov A, et al. Reactive electric-discharge sintering of TiN–TiB_2. Powder Metall Metal Ceram 2007;46(11–12):525–32.
[12] Moshtaghioun BM, Gómez-García D, Domínguez-Rodríguez A. Spark plasma sintering of titanium nitride in nitrogen: does it affect the sinterability and the mechanical properties? J Eur Ceram Soc 2018;38(4):1190–6.
[13] Xue J-X, Liu H-T, Tang Y, Xu C-M, Zhang G-J. Effect of sintering atmosphere on the densification behavior of hot pressed TiN ceramics. Ceram Int 2013;39(7):8531–5.
[14] Kim W, Roh K-M, Lim J-W, Oh H-S, Shon I-J. The effect of ball milling on the mechanical properties of TiN consolidated by pulsed current activated sintering. J Alloys Compds 2013;574:260–5.
[15] Akin I, Hotta M, Sahin FC, Yucel O, Goller G, Goto T. Microstructure and densification of ZrB_2–SiC composites prepared by spark plasma sintering. J Eur Ceram Soc 2009;29(11):2379–85.
[16] Zeng W, Gan X, Li Z, Zhou K. Effect of TiC addition on the microstructure and mechanical properties of TiN-based cermets. Ceram Int 2017;43(1):1092–7.
[17] Bläß U, et al. Bulk titanium nitride ceramics – significant enhancement of hardness by silicon nitride addition, nanostructuring and high pressure sintering. J Eur Ceram Soc 2015;35(10):2733–44.
[18] Radajewski M, et al. Microstructure and mechanical properties of bulk TiN–AlN composites processed by FAST/SPS. Ceram Int 2016;42(8):10220–7.
[19] Kuwahara H, Mazaki N, Takahashi M, Watanabe T, Yang X, Aizawa T. Mechanical properties of bulk sintered titanium nitride ceramics. Mater Sci Eng A 2001;319:687–91.
[20] Shon I-J. Enhanced mechanical properties of TiN–graphene composites rapidly sintered by high-frequency induction heating. Ceram Int 2017;43(1):890–6.
[21] Namini AS, Azadbeh M, Asl MS. Effects of in-situ formed TiB whiskers on microstructure and mechanical properties of spark plasma sintered Ti-B_4C and Ti-TiB_2 composites. Sci Iran Trans B Mech Eng 2018;25(2):762–71.
[22] Asl MS. A statistical approach towards processing optimization of ZrB_2–SiC–graphite nanocomposites. Part I: relative density. Ceram Int 2018;44(6):6935–9.
[23] Asl MS, Zamharir MJ, Ahmadi Z, Parvizi S. Effects of nano-graphite content on the characteristics of spark plasma sintered ZrB_2–SiC composites. Mater Sci Eng A 2018;716:99–106.

[24] Asl MS, Namini AS, Motallebzadeh A, Azadbeh M. Effects of sintering temperature on microstructure and mechanical properties of spark plasma sintered titanium. Mater Chem Phys 2018;203:266–73.
[25] Asl MS. Microstructure, hardness and fracture toughness of spark plasma sintered ZrB_2–SiC–Cf composites. Ceram Int 2017;43(17):15047–52.
[26] Asl MS, Ahmadi Z, Parvizi S, Balak Z, Farahbakhsh I. Contribution of SiC particle size and spark plasma sintering conditions on grain growth and hardness of TiB2 composites. Ceram Int 2017;43(16):13924–31.
[27] Namini AS, Ahmadi Z, Babapoor A, Shokouhimehr M, Asl MS. Microstructure and thermomechanical characteristics of spark plasma sintered TiC ceramics doped with nano-sized WC. Ceram Int 2019;45(2):2153–60.
[28] Akhlaghi M, Tayebifard SA, Salahi E, Asl MS. Spark plasma sintering of TiAl–Ti_3AlC_2 composite. Ceram Int 2018;44(17):21759–64.
[29] Germi MD, Mahaseni ZH, Ahmadi Z, Asl MS. Phase evolution during spark plasma sintering of novel Si_3N_4-doped TiB_2–SiC composite. Mater Charact 2018;145:225–32.
[30] Wyzga P, Jaworska L, Bucko MM, Bonarski J, Putyra P, Figiel P. TiN–TiB_2 composites prepared by various sintering techniques. Int J Refract Metals Hard Mater 2013;41:571–6.
[31] Kitiwan M, Ito A, Goto T. Spark plasma sintering of TiN–TiB_2 composites. J Eur Ceram Soc 2014;34(2):197–203.
[32] Kitiwan M, Ito A, Goto T. Spark plasma sintering of TiN–TiB_2–hBN composites and their properties. Ceram Int 2015;41(3):4498–503.
[33] Wang K, Krstic V. Reaction sintering of TiN–TiB_2 ceramics. Acta Mater 2003;51(6):1809–19.
[34] Ouyang J, Yang Z, Liu Z, Liang X. Friction and wear properties of reactive hot-pressed TiB_2–TiN composites in sliding against Al_2O_3 ball at elevated temperatures. Wear 2011;271(9–10):1966–73.
[35] Yang Z-L, Ouyang J-H, Liu Z-G. Isothermal oxidation behavior of reactive hot-pressed TiN–TiB_2 ceramics at elevated temperatures. Mater Des 2011;32(1):29–35.
[36] Ajayan PM, Schadler LS, Giannaris C, Rubio A. Single-walled carbon nanotube–polymer composites: strength and weakness. Adv Mater 2000;12(10):750–3.
[37] Munir ZA, Quach DV, Ohyanagi M. Electric current activation of sintering: a review of the pulsed electric current sintering process. J Am Ceram Soc 2011;94(1):1–19.
[38] Chicardi E, et al. Toughening of complete solid solution cermets by graphite addition. Chem Eng J 2015;267:297–305.
[39] Mimoto T, Nakanishi N, Umeda J, Kondoh K. Mechanical Properties and Strengthening mechanism of pure Ti powder composite material reinforced with carbon nano particles. Trans JWRI 2011;40(2):63–8.
[40] Lohse B, Calka A, Wexler D. Raman spectroscopy as a tool to study TiC formation during controlled ball milling. J Appl Phys 2005;97(11):114912.
[41] Ye L, Quan M. Synthesis of nanocrystalline TiC powders by mechanical alloying. Nanostruct Mater 1995;5(1):25–31.
[42] Dorofeev G, et al. Mechanochemical interaction of titanium powder with organic liquids. Int J Hydrogen Energy 2014;39(18):9690–9.
[43] Xiang J, et al. Mechanochemically activated synthesis of zirconium carbide nanoparticles at room temperature: a simple route to prepare nanoparticles of transition metal carbides. J Eur Ceram Soc 2011;31(8):1491–6.
[44] Razavi M, Rahimipour MR, Rajabi-Zamani AH. Synthesis of nanocrystalline TiC powder from impure Ti chips via mechanical alloying. J Alloys Compds 2007;436(1–2):142–5.
[45] Lohse B, Calka A, Wexler D. Synthesis of TiC by controlled ball milling of titanium and carbon. J Mater Sci 2007;42(2):669–75.
[46] Yuan Q, Zheng Y, Yu H. Mechanism of synthesizing nanocrystalline TiC in different milling atmospheres. Int J Refract Metals Hard Mater 2009;27(4):696–700.
[47] Dong P, Wang Z, Wang W, Chen S, Zhou J. Understanding the spark plasma sintering from the view of materials joining. Scr Mater 2016;123:118–21.
[48] Yang J, Aizawa T, Yamamoto A, Ohta T. Thermoelectric properties of n-type $(Bi_2Se_3)_x(Bi_2Te_3)_{1-x}$ prepared by bulk mechanical alloying and hot pressing. J Alloys Compds 2000;312(1–2):326–30.
[49] Banaszek K, Januszewicz B, Wołowiec E, Klimek L. Complex XRD and XRF characterization of TiN-TiCN-TiC surface coatings for medical applications. In: Solid state phenomena, vol. 225. Trans Tech Publ.; 2015. p. 159–68.
[50] Devia D, Restrepo J, Ruden A, González J, Sequeda F, Arango P. The tribological characteristics of TiN, TiC, TiC/TiN films prepared by reactive pulsed arc evaporation technique. In: Society of vacuum coaters, vol. 505; 2009. p. 32–6.
[51] Falodun OE, Obadele BA, Oke SR, Ige OO, Olubambi PA. Effect of TiN and TiCN additions on spark plasma sintered Ti–6Al–4V. Partic Sci Technol 2018:1–10.
[52] Kim K, Suh C, Murakami R, Chung C. Effect of intrinsic properties of ceramic coatings on fatigue behavior of Cr–Mo–V steels. Surf Coat Technol 2003;171(1–3):15–23.
[53] Hackett K, Verhoef S, Cutler RA, Shetty DK. Phase constitution and mechanical properties of carbides in the Ta–C system. J Am Ceram Soc 2009;92(10):2404–7.
[54] Peng Y, Miao H, Peng Z. Development of TiCN-based cermets: mechanical properties and wear mechanism. Int J Refract Metals Hard Mater 2013;39:78–89.
[55] Akinribide OJ, Mekgwe GN, Obadele BA, Ajibola OO, Akinwamide SO, Olubambi PA. Microstructural and phase evolution of spark plasma sintering of graphitized Ti (C0.9N0.1) composites. Int J Refract Metals Hard Mater 2019;78:164–9.
[56] Laoui T, Zou H, Van der Biest O. Analytical electron microscopy of the core/rim structure in titanium carbonitride cermets. Int J Refract Metals Hard Mater 1992;11(4):207–12.
[57] Rafaja D, Dopita M, Masimov M, Klemm V, Wendt N, Lengauer W. Analysis of local composition gradients in the hard-phase grains of cermets using a combination of X-ray diffraction and electron microscopy. Int J Refract Metals Hard Mater 2008;26(3):263–75.
[58] Cutard T, Viatte T, Feusier G, Benoit W. Microstructure and high temperature mechanical properties of TiC0.7N0.3Mo2CNi cermets. Mater Sci Eng A 1996;209(1–2):218–27.
[59] Arya A, Carter EA. Structure, bonding, and adhesion at the TiC (100)/Fe (110) interface from first principles,. J Chem Phys 2003;118(19):8982–96.
[60] Xiong W. On the mechanism of phase interface combination in Ti (C, N) based cermet. J-Huazhong Univ Sci Technol Chin Ed 1995;23:28–32.